
This is an electronic reprint of the original article.
This reprint may differ from the original in pagination and typographic detail.

Gan, Tian; Song, Hexuan; Fan, Xinqiang; Liu, Ye; Liu, Shouqing; Zhao, Yicheng; Li, Yongdan

A rational design of highly active and coke-resistant anode for methanol-fueled solid oxide fuel cells with Sn doped Ni-Ce_{0.8}Sm_{0.2}O_{2-δ}

Published in:
Chemical Engineering Journal

DOI:
[10.1016/j.cej.2022.140692](https://doi.org/10.1016/j.cej.2022.140692)

Published: 01/01/2023

Document Version
Publisher's PDF, also known as Version of record

Published under the following license:
CC BY

Please cite the original version:
Gan, T., Song, H., Fan, X., Liu, Y., Liu, S., Zhao, Y., & Li, Y. (2023). A rational design of highly active and coke-resistant anode for methanol-fueled solid oxide fuel cells with Sn doped Ni-Ce_{0.8}Sm_{0.2}O_{2-δ}. *Chemical Engineering Journal*, 455, Article 140692. <https://doi.org/10.1016/j.cej.2022.140692>

This material is protected by copyright and other intellectual property rights, and duplication or sale of all or part of any of the repository collections is not permitted, except that material may be duplicated by you for your research use or educational purposes in electronic or print form. You must obtain permission for any other use. Electronic or print copies may not be offered, whether for sale or otherwise to anyone who is not an authorised user.



A rational design of highly active and coke-resistant anode for methanol-fueled solid oxide fuel cells with Sn doped Ni-Ce_{0.8}Sm_{0.2}O_{2-δ}

Tian Gan^{a,b,c}, Hexuan Song^{b,c}, Xinqiang Fan^{b,c}, Ye Liu^{b,c}, Shouqing Liu^a, Yicheng Zhao^{b,c,*}, Yongdan Li^{b,c,d,*}

^a School of Chemistry and Life Science, Suzhou University of Science and Technology, Suzhou 215009, China

^b State Key Laboratory of Chemical Engineering (Tianjin University), Tianjin Key Laboratory of Applied Catalysis Science and Technology, School of Chemical Engineering and Technology, Tianjin University, Tianjin 300072, China

^c Collaborative Innovation Center of Chemical Science and Engineering (Tianjin), Tianjin 300072, China

^d Department of Chemical and Metallurgical Engineering, School of Chemical Engineering, Aalto University, Kemistintie 1, Espoo, P.O. Box 16100, FI-00076 Aalto Finland

ARTICLE INFO

Keywords:

Ni-Sn intermetallic compounds
Doped ceria
Methanol fuel
Anode
Solid oxide fuel cell

ABSTRACT

A crucial challenge in the commercialization of Ni-based materials as the anode of solid oxide fuel cell is the fast voltage drop due to carbon deposition and structural degradation during cell operation. Herein, Sn-doped Ce_{0.8}Sm_{0.2}O_{2-δ} (SDC) supported Sn-Ni alloy anode is rationally designed and prepared, via a simple and convenient dual-modification strategy. The substitution of Sn of Ce in the oxide phase enhances the mobility of lattice oxygen in SDC. Meanwhile, Sn exsolves partially from the oxide phase and forms Ni₃Sn and Ni₃Sn₂ intermetallic compounds with Ni after reduction. The composite anode thus formed achieves unprecedented activity in the electrochemical oxidation of H₂ and CH₃OH. The maximum power densities of a cell supported by 500 μm-thick Ce_{0.8}Sm_{0.2}O_{2-δ}-carbonate electrolyte layer with the Ni-Ce_{0.7}Sn_{0.1}Sm_{0.2}O_{2-δ} (Ni-SSn₁₀DC) anode reach 1.99 and 2.11 W cm⁻² at 700 °C, respectively for using H₂ and methanol as fuels. The doping of Sn also remarkably enhances the coking resistance of the anode. This work opens a path on the design of high-performance SOFC anode.

1. Introduction

Solid oxide fuel cells (SOFCs) are considered as one of the most efficient electrochemical energy-conversion devices due to their high energy efficiency, low pollutant emission and high flexibility to utilize various fuels such as hydrogen, syngas and hydrocarbons [1–3]. Readily available hydrocarbon fuels with a low cost and good security are considered as promising alternatives to conventional H₂ fuel for fuel cells [4]. Furthermore, liquid renewable hydrocarbon fuels such as methanol has high volume energy densities (1.6 × 10⁴ kJ m⁻³), which is beneficial to fuel storage and the mobile applications at ambient pressure and temperature. Moreover, unlike other heavier alcohols like ethanol with the C–C bond in the molecular structures, the cleavage of C–H bonds is much easier for methanol through methanol thermal decomposition or steam reforming of methanol [5–7]. However, the utilization of hydrocarbon fuels in SOFC is hindered by serious carbon deposition on anode catalyst and the sluggish anode kinetics [8].

Ni-based cermet with a high electrical conductivity is the most widely used anode material in SOFC research. Besides external and internal reforming, which first transforms the hydrocarbon feed to syngas, much effort has been focused on enhancing the activity and the resistance to coking of the Ni-based anode materials for the direct electrochemical conversion of hydrocarbon fuels. Cu with a high coking resistance has been used to replace Ni fully or partially, which leads to a low catalytic activity [9]. Yoon and Manthiram [10] found that the incorporation of 1 atom% W to Ni brings in surface hydroxyl groups through the reaction with water vapor, which facilitates the oxidation of carbon deposited. The addition of BaO and NbO_x has similar effects [11–13]. The alloying of Ni with other metals, such as Co [14,15], Mo [16] and Fe [17,18], improves the anode activity and suppresses carbon deposition. Among the possible alternative alloys, Ni-Sn is potentially an excellent candidate for the anode catalyst [19,20]. The computation models suggest that Ni-Sn is more carbon-tolerant than Ni [21]. However, Li et al. [22] found that the addition of Sn in Ni decreases the anode

* Corresponding authors.

E-mail addresses: zhaoyicheng@tju.edu.cn (Y. Zhao), yongdan.li@aalto.fi (Y. Li).

<https://doi.org/10.1016/j.cej.2022.140692>

Received 15 July 2022; Received in revised form 12 October 2022; Accepted 27 November 2022

Available online 29 November 2022

1385-8947/© 2022 The Authors. Published by Elsevier B.V. This is an open access article under the CC BY license (<http://creativecommons.org/licenses/by/4.0/>).

activity slightly while improving the coking resistance remarkably with CH₄ as fuel. Notably, intermetallic compounds (IMCs) gradually attracted more attention because they exhibit unique catalytic properties. Cabot et al. [23] prepared NiSn NPs with controlled stoichiometry and achieved excellent performance towards methanol oxidation reaction, meanwhile, significantly improved stability compared to single metal nickel. However, the effect of NiSn IMCs, as active sites on the anode of methanol fueled SOFC, on the catalytic performance of the anode has not been reported.

The recent research on cermet anodes mainly focuses on the metal catalysts. Nevertheless, the ceramic support providing oxygen ions also have remarkable influence on the activity and coking resistance of the cermet anodes with hydrocarbon fuels [24,25]. The activity of a Cu-based anode with doped ceria as the support is much higher than that with yttria stabilized zirconia (YSZ) as support when CH₄ is used as the fuel, attributing to the high oxygen storage capacity (OSC) of ceria [9]. The activity and coking resistance of cermet anode with Ce_{0.8}Sm_{0.2}O_{1.9} (SDC) as support are enhanced when Sm is partially substituted with other rare earth metals such as La, Pr and Nd due to the improved activity of surface oxygen species [26,27]. Among the very few examples in the literature, Sn doped CeO₂ was used as a support in CO oxidation [28,29]. Sn improves the reducibility and OSC of CeO₂, bringing about a high catalytic activity. However, Sn doped SDC has not yet been tested as anode material in SOFC.

In this work, Sn doped SDC (Ce_{0.8-x}Sn_xSm_{0.2}O_{2-δ}, x = 0–0.15, SSnDC) is examined as the support in Ni-based cermet anode. We found that excessive Sn exsolves partially from the oxide phase and forms intermetallic compounds with Ni after reduction. The effects of Sn in both metal and the oxide phases are investigated. The dual-modified Ni-SDC anode material with Sn doping shows enhanced performance and stability with methanol as the fuel.

2. Experimental

2.1. Preparation of anode powders

SDC, Ce_{0.75}Sn_{0.05}Sm_{0.2}O_{2-δ} (SSn₅DC), Ce_{0.70}Sn_{0.10}Sm_{0.2}O_{2-δ} (SSn₁₀DC) and Ce_{0.65}Sn_{0.15}Sm_{0.2}O_{2-δ} (SSn₁₅DC) powders were synthesized via a hydrothermal procedure [30,31]. All of the chemicals (A.R. in purity) were purchased from Shanghai Aladdin Bio-Chem Technology Co., Ltd. Stoichiometric Ce(NO₃)₃·6H₂O, SnCl₄·5H₂O and Sm(NO₃)₃·6H₂O were dissolved in deionized water to form a solution with a total metal ion concentration of 0.15 mol L⁻¹. Urea was subsequently added to the solution under constant stirring to reach a concentration of 1 mol L⁻¹. Then the precursor solution was transferred into a hydrothermal reactor and kept at 140 °C for 5 h. The precipitate was washed with deionized water until no Cl⁻ was detected with 0.1 mol L⁻¹ AgNO₃ solution. The powder obtained was dried at 100 °C for 12 h and finally calcined in air at 700 °C for 2 h.

NiO-SSn_xDC (x = 0, 5, 10 and 15) powders with a Ni loading amount of 10 wt% were prepared through an incipient wetness impregnation technique with a Ni(NO₃)₂·6H₂O aqueous solution. Then the powders were dried at room temperature overnight and calcined subsequently at 700 °C in air for 2 h. The sample was reduced in pure H₂ at 700 °C for 2 h for characterization and are marked as Ni-SSn_xDC. For comparison, a sample, denoted as Sn@Ni-SDC, was prepared as follows. Sn, equivalent to 50 wt% Sn in Ni-SSn₁₀DC, was added into the NiO-SDC powder via impregnation with an aqueous solution of SnCl₄·5H₂O.

2.2. Characterization

A D8 Focus diffractometer (Bruker Corp., Cu Kα radiation, 40 kV and 200 mA) X-ray was used to record the diffraction (XRD) patterns at a scanning rate of 1° min⁻¹. The microstructure of the samples was observed using a transmission electron microscope (TEM, JEM-200F, JEOL Inc., Japan). High-angle annular dark-field scanning TEM

(HAADF-STEM) and energy-dispersive X-ray (EDX) analysis were carried out to mapping the element distributions. The surface property of the samples was analyzed with an ESCALAB 250 Xi X-ray photoelectron spectrometer (XPS, K-Alpha+, Thermo Fisher Scientific) using Al-Kα (hν = 1486.6 eV) as the X-ray source. The spectra obtained were referenced to the C 1 s binding energy (284.8 eV).

The activity of oxygen species in the samples was evaluated with CH₃OH temperature-programmed surface reaction (CH₃OH-TPSR) in a quartz tube reactor. 80 mg of powder was reduced in hydrogen at 700 °C for 2 h. After cooling to 150 °C, the sample was treated in pure O₂ (30 mL min⁻¹) for 30 min and was purged subsequently with Ar (30 mL min⁻¹) at the same temperature for another 30 min to sweep the weakly absorbed oxygen. Then about 10 vol% gasified CH₃OH was added in Ar by bubbling Ar through liquid CH₃OH at room temperature. The reactor was heated from 150 to 800 °C at a heating rate of 5 °C min⁻¹, and the oxidation of CH₃OH was monitored with measuring the amount of CO₂ produced with an online mass spectrometer (HPR20, Hidden Analytic Ltd.). The reduced anode powder was treated with gasified anhydrous methanol (150 mL min⁻¹, STP) at 700 °C for 4 h. The carbon deposited was observed with a scanning electron microscope (SEM, S-4800, Hitachi, Japan), and its amount was measured with thermogravimetric analysis (TGA) in oxygen atmosphere using a thermal analyser (NETZSCH STA449, Germany).

2.3. Cell fabrication and test

70 wt% SDC and 30 wt% (Li_{0.67}Na_{0.33})₂CO₃ composite was used as the electrolyte material [32], which was uniaxially pressed into disk-shaped pellets at 500 MPa and then sintered at 700 °C for 2 h. The diameter and the thickness of the electrolyte layer were 13 mm and 500 μm, respectively. The anode powder was mixed with an organic binder (V006, Heraeus Ltd.) to make a slurry, which was screen-printed on both sides of the electrolyte pellets, and subsequently calcined at 700 °C for 2 h to form symmetric cells. The geometrical area of the electrode was 0.64 cm², and Ag paste was used as the current collector. The electrode layers were reduced in H₂ at 700 °C for 2 h, and then the electrochemical impedance spectra (EIS) of the symmetric cell were recorded with an electrochemical workstation (VERSASTAT 3, Ametek) under various H₂ partial pressures (with Ar as the balance gas).

Electrolyte-supported single cells were fabricated via a similar screen-printing process [18]. The cathode consisted of 70 wt% composite electrolyte and 30 wt% lithiated NiO, which was screen-printed on one side of the electrolyte pellet. The anode slurry was printed on the other side of the pellet, followed by calcined at 700 °C for 2 h to form single cells. The anode was reduced in H₂ at 700 °C for 2 h, and then the performance of the cell was measured using the electrochemical workstation with dry hydrogen and gasified anhydrous methanol (100 mL min⁻¹, STP) as the fuels and O₂ (30 mL min⁻¹, STP) as the oxidant.

3. Results

3.1. Electrochemical performance

The *I-V* and *I-P* characteristics of the single cells with dry H₂ as the fuel at 700 °C are presented in Fig. 1a. The open circuit voltages (OCV) of the cells are between 1.00 and 1.12 V. The maximum power density (*P*_{max}) of the cells with Ni-SDC, Ni-SSn₅DC, Ni-SSn₁₀DC and Ni-SSn₁₅DC anodes are 0.53, 1.15, 1.93 and 1.62 W cm⁻², respectively. When the temperature drops to 650, 600 and 550 °C, the *P*_{max} of the cell with the Ni-SSn₁₀DC anode decreases to 1.56, 0.97 and 0.61 W cm⁻², respectively (Fig. S1a). When methanol is used as the fuel, the OCVs are in the range of 1.00–1.08 V (Fig. 1b), and the cell with the Ni-SSn₁₀DC anode shows the highest *P*_{max} of 2.11 W cm⁻², much higher than that of the cell with the Ni-SDC anode (0.78 W cm⁻²). When the temperature drops to 650, 600 and 550 °C, the *P*_{max} of the cell with the Ni-SSn₁₀DC anode decreases to 1.74, 1.18 and 0.83 W cm⁻², respectively (Fig. 1c), which is

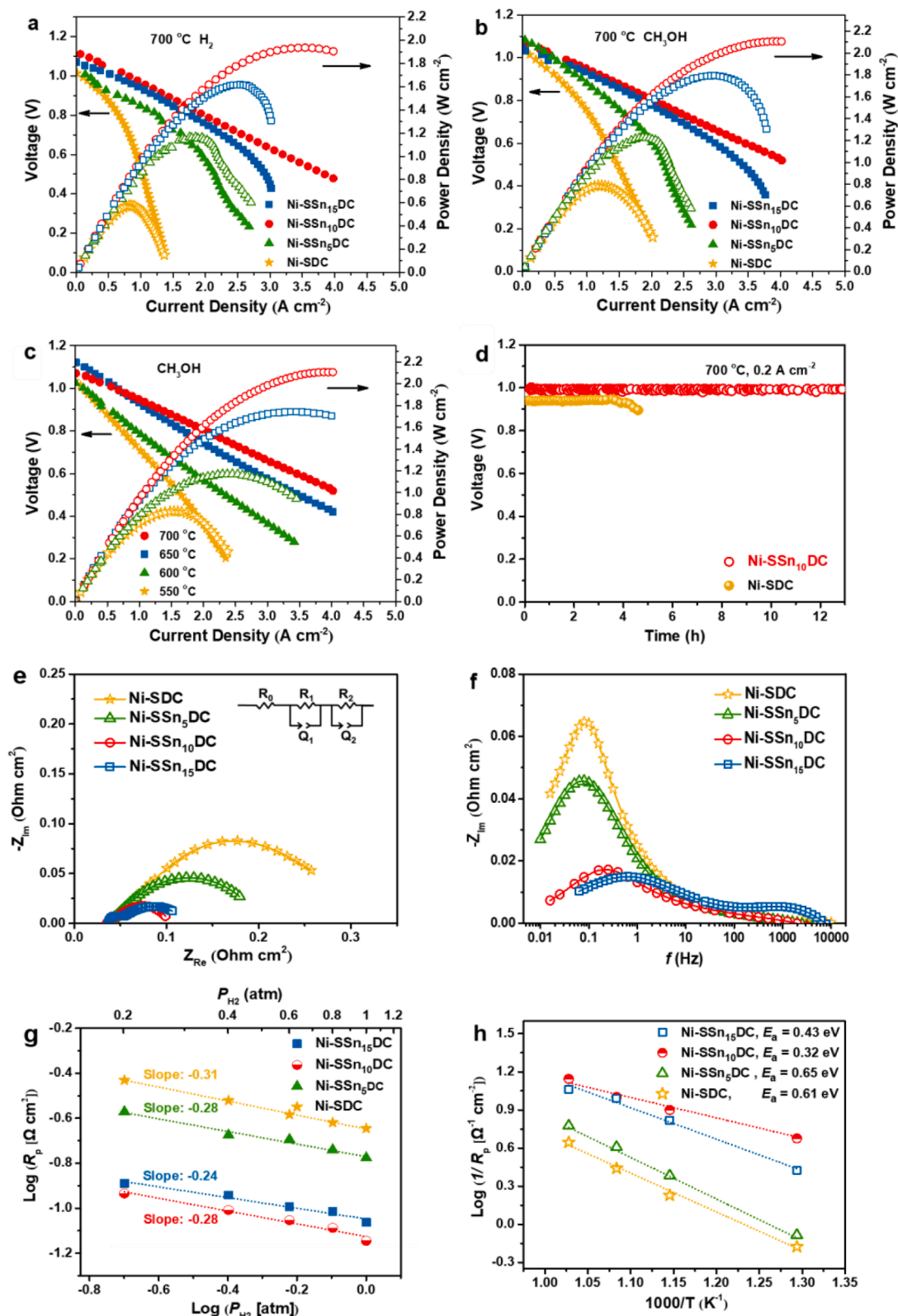


Fig. 1. *I-V* and *I-P* curves of single cells with various anodes fed with (a) dry hydrogen and (b) methanol at 700 °C; (c) *I-V* and *I-P* curves of the cell with Ni-SSn₁₀DC anode at various temperatures with methanol as the fuel; (d) Chronopotentiometry measurement result of two single cells with Ni-SSn₁₀DC and Ni-SDC anodes fed with methanol at 700 °C. (e) Nyquist and (f) Bode plots of the symmetric cells with H₂ as the fuel at 700 °C; (g) *R_p* of the symmetric cells versus *P_{H₂}* at 700 °C; (h) Arrhenius plots of *R_p* of the symmetric cells. All the impedances have been divided by two.

similar to the trend of P_{\max} obtained at different temperatures with dry H_2 as the fuel. The corresponding impedance spectra at the open circuit condition are presented in Fig. S1b, c. The good performance of the cell in the intermediate temperature range is attributed to the high catalytic activity and the low activation energies (E_a) of the Ni-SSn₁₀DC anode. Fig. 1d shows the short-term stability of the single cells with methanol as the fuel at a constant current density of 0.2 A cm⁻² at 700 °C. The cell with the Ni-SDC anode exhibits a steady output voltage in the first 4 h, which then drops gradually probably due to the coking on the anode. On the contrary, the output voltage of the cell with the Ni-SSn₁₀DC anode is stable for more than 12 h attributed to the improvement of the resistance to carbon deposition of the anode with Sn doping.

The EIS curves of the symmetric cells with H_2 and methanol at both sides at 700 °C are presented in Fig. 1e and Fig. S1d. The data are fitted with the equivalent circuit $R_0(R_1Q_1)(R_2Q_2)$, in which R_0 , R_1 and R_2 are resistances, while Q_1 and Q_2 are constant phase elements. The ohmic resistances of the cells shown as the intercepts of the Nyquist curves on the real axis in high frequency region are similar. The anode polarization resistances (R_p) reflected by the arcs show an order of Ni-SDC > Ni-SSn₅DC > Ni-SSn₁₅DC > Ni-SSn₁₀DC.

The Bode plots of the cells are shown in Fig. 1f, which can be roughly divided into a high frequency (HF, 10⁴–10¹ Hz) region and a low frequency (LF, 10¹–10⁻² Hz) region. The R_p in the LF region decreases remarkably with the doping of Sn in the anode support. Ni-SDC, Ni-SSn₅DC and Ni-SSn₁₀DC anodes exhibit similar R_p in the HF region, while that of the Ni-SSn₁₅DC anode is slightly larger.

The EIS results of the symmetric cells under various hydrogen partial pressures (P_{H_2}) are plotted in Fig. S1e, in which the ohmic resistances are deduced for a better comparison. The R_p of all the anodes increase with the decrease of P_{H_2} , and linear relationships between Log R_p and Log P_{H_2} are observed (Fig. 1g). The slope values for Ni-SSn_xDC are 0.24 ~ 0.31.

The Arrhenius plots of the R_p of the anodes are presented in Fig. 1h. The E_a of the electrochemical oxidation of H_2 on Ni-SDC and Ni-SSn₅DC anodes are 0.61–0.65 eV. The Ni-SSn₁₀DC anode shows the lowest E_a of 0.32 eV attributed to the acceleration of the surface steps, while the E_a of Ni-SSn₁₅DC increases to 0.43 eV due to the suppression of the bulk conduction of O²⁻.

3.2. Characterization

The cross-sectional SEM images of the single cell with Ni-SSn₁₀DC anode before test are shown in Fig. 2a and Fig. S2. The thicknesses of the anode, the electrolyte and the cathode layers are about 30, 500 and 40 μ m, respectively. The anode surface exhibits a fine and uniform porous microstructure (Fig. 2b).

The hydrothermally synthesized SDC powder shows a face-centered cubic fluorite structure (JCPDS#075–0158, Fig. S3a). With the partial substitution of Sn for Ce, the fluorite structure is maintained. Meanwhile, the XRD peaks shift gradually to higher angles, indicating the

contraction of SDC lattice with the incorporation of Sn since Sn⁴⁺ (0.81 Å) is smaller than Ce⁴⁺ (0.97 Å) [33,34]. Furthermore, the characteristic peaks of SnO₂ (JCPDS#041–1445) is observed in the XRD pattern of SSn₁₅DC, implying a limited solubility of Sn in SDC [35,36]. The XRD results without obvious SnO₂ peaks probably are caused by the low amount of SnO₂ phase and its uniform distribution on the support. SDC and Ni (JCPDS#087–0712) phases are found in Ni-SDC after reduction (Fig. 3a). With the addition of Sn in the SDC phase, the Ni peaks are weakened remarkably, while Ni₃Sn and Ni₃Sn₂ phases are observed, indicating the partial exsolution of Sn and the formation of intermetallic compounds during the reduction. Ni-SSn₁₀DC has the strongest Ni₃Sn peaks, while more Ni₃Sn₂ phase is found in Ni-SSn₁₅DC. Ni₃Sn and Ni₃Sn₂ phases are also formed in the Sn@Ni-SDC after reduction. Rietveld refinement of XRD data for the Ni-SSn_xDC anode is carried out and the results are shown in Fig. 3b and Fig. S2c–f. Fig. S4 depicts the unit cell structure of SSn_xDC, with a cubic fluorite structure, drawn using the VESTA software. All materials have a tetragonal structure (space group *I4/mmm*). The lattice parameters of Ni-SSn₁₀DC are $a = b = 8.655$ Å and $c = 5.500$ Å. These parameters are slightly smaller than those of Ni-SDC, which were $a = b = 8.752$ Å and $c = 5.536$ Å. These refinement results demonstrate the lattice volume shrinkage after Sn doping.

The TEM micrograph of the NiO-SSn₁₀DC anode powder before reduction is shown in Fig. 3c, revealing the nanoparticles with the size of 10–20 nm. The lattice fringes corresponding to NiO, SDC and SnO₂ are observed in the HRTEM image (Fig. 3d). After reduction, the nanoparticles of Ni, Ni₃Sn and Ni₃Sn₂ are formed (Fig. 3e–g). The HAADF-STEM image and the corresponding EDX elemental mappings of the reduced Ni-SSn₁₀DC anode is shown in Fig. 3h. Ni exists in all the nanoparticles, while Ce is found only in the SDC phase. On the contrary, Sn is distributed in the whole anode, further proving the partial exsolution of Sn from SDC phase and the formation of Ni-Sn intermetallic compounds. The TEM results are consistent with the XRD characterization. The structure of the Ni-SSn_xDC anode material is illustrated in Fig. 3i.

The surface chemical states of the anode samples were further investigated with a XPS technique. Fig. 4 shows the XPS survey spectra and the corresponding fitting curves of the Ni 2p and Sn 3d spectra after reduction. The deconvoluted peaks at about 852.3 and 854.0 eV are attributed to Ni⁰ and Ni²⁺, respectively (Fig. 4a) [37,38]. Ni²⁺ is probably formed from the quick reoxidation of metallic Ni on the surface of the reduced anodes before the XPS test [39,40]. Meanwhile, the binding energy of Ni⁰ decreases slightly with the addition of Sn, indicating the electron transfer from Sn to Ni in Ni₃Sn and Ni₃Sn₂ [41,42]. The Sn 3d spectrum of the Ni-SSn_xDC in Fig. 4b could be deconvoluted into Sn⁰, Sn²⁺ and Sn⁴⁺ components, revealing the coexistence of Sn, Sn²⁺ and Sn⁴⁺ species on the surface of Ni-SSn_xDC.

The CH₃OH-TPSR results of the SSn_xDC composite oxide powders are presented in Fig. 5a. The weak CO₂ peaks at about 300 °C are due to the reaction between CH₃OH and oxygen species adsorbed weakly on the

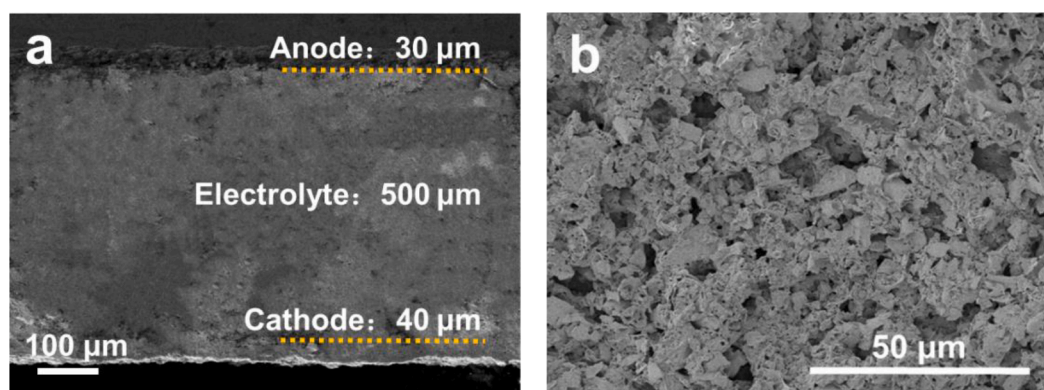


Fig. 2. SEM images of (a) cross-section of the cell with NiO-SSn₁₀DC anode and (b) NiO-SSn₁₀DC anode surface.

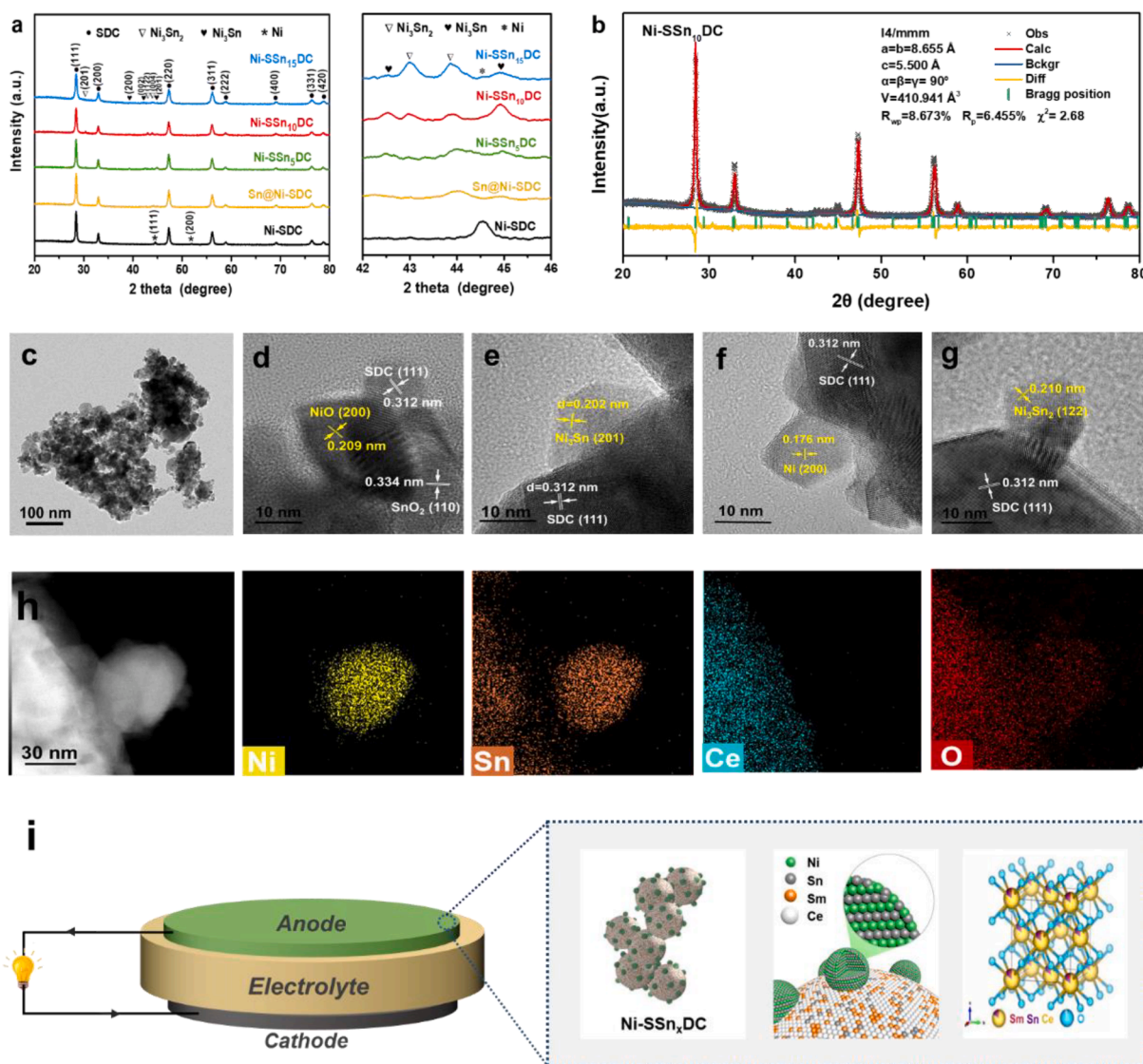


Fig. 3. (a) XRD patterns of Ni-SSn_xDC anode after reduction. (b) Rietveld refined profiles of Ni-SSn₁₀DC powder. (c) TEM micrographs of NiO-SSn₁₀DC powder before reduction; HRTEM images of NiO-SSn₁₀DC powder before (d) and after (e-g) reduction. (h) HAADF-STEM image of reduced Ni-SSn₁₀DC anode powder and the corresponding EDX elemental mappings. (i) Schematic view of the Ni-SSn_xDC anode structure.

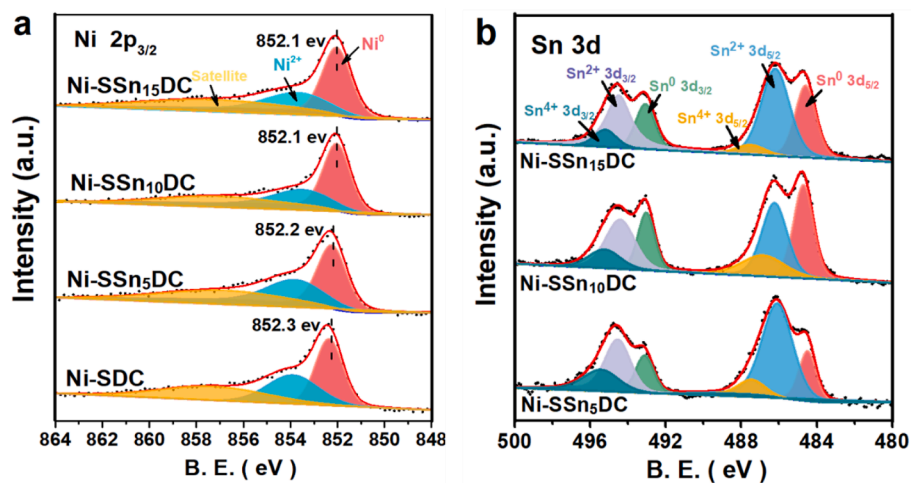


Fig. 4. XPS spectra of (a) Ni 2p_{3/2} and (b) Sn 3d of the reduced anode samples.

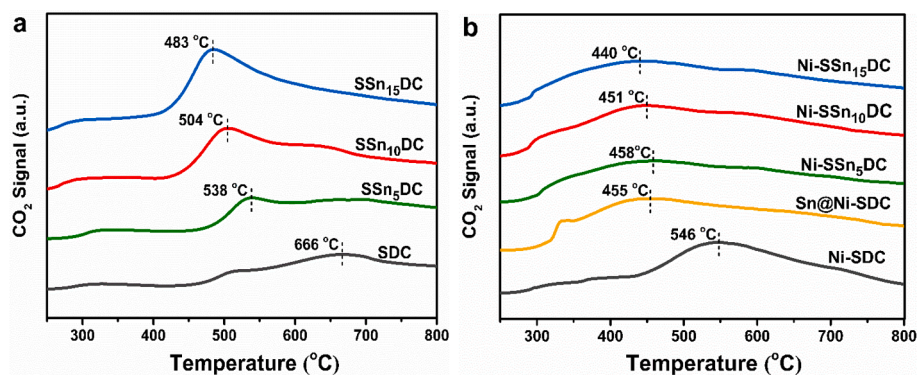


Fig. 5. CH_3OH -TPSR results of (a) SSn_xDC supports and (b) reduced anode powders.

surface of the samples, while the strong peaks in 400–700 °C correspond to the oxidation of CH_3OH by lattice oxygens [26]. The oxidation of CH_3OH on SDC reaches the highest rate at about 666 °C. With the increase of Sn content in SDC, the oxidation temperature of CH_3OH decreases gradually, indicating that the partial substitution of Sn for Ce enhances the activity of lattice oxygen in SDC. The CH_3OH -TPSR curves of the $\text{Ni-SSn}_x\text{DC}$ anode powders after reduction are shown in Fig. 5b. The oxidation temperature of CH_3OH on Ni-SDC (546 °C) is much lower than that on SDC, and the impregnation of Sn (Sn@Ni-SDC) further decreases the oxidation temperature significantly, demonstrating that the formation of Ni-Sn intermetallic compounds improves the catalytic activity towards CH_3OH oxidation. These results suggest that the dual-

modified Ni-SDC with Sn are more favorable to the CH_3OH oxidation process.

The SEM images of the anode powders after carbon deposition are shown in Fig. 6. The surface of Ni-SDC is closely packed by filamentous carbon (Fig. 6a), while negligible carbon is found on $\text{Ni-SSn}_{10}\text{DC}$ (Fig. 6b). The TGA curves of the samples in the oxygen atmosphere are presented in Fig. 6c. The weight loss in 400–650 °C reflects the oxidation of carbon deposits. The weight losses of Ni-SDC , $\text{Ni-SSn}_5\text{DC}$, $\text{Ni-SSn}_{10}\text{DC}$ and $\text{Ni-SSn}_{15}\text{DC}$ are 27, 4.5, 2.4 and 1.8 wt%, respectively. The addition of Sn results in the enhancement of oxygen activity of the support and the formation of Ni_3Sn and Ni_3Sn_2 , both bring about the remarkable improvement of the resistance to carbon deposition [43–45].

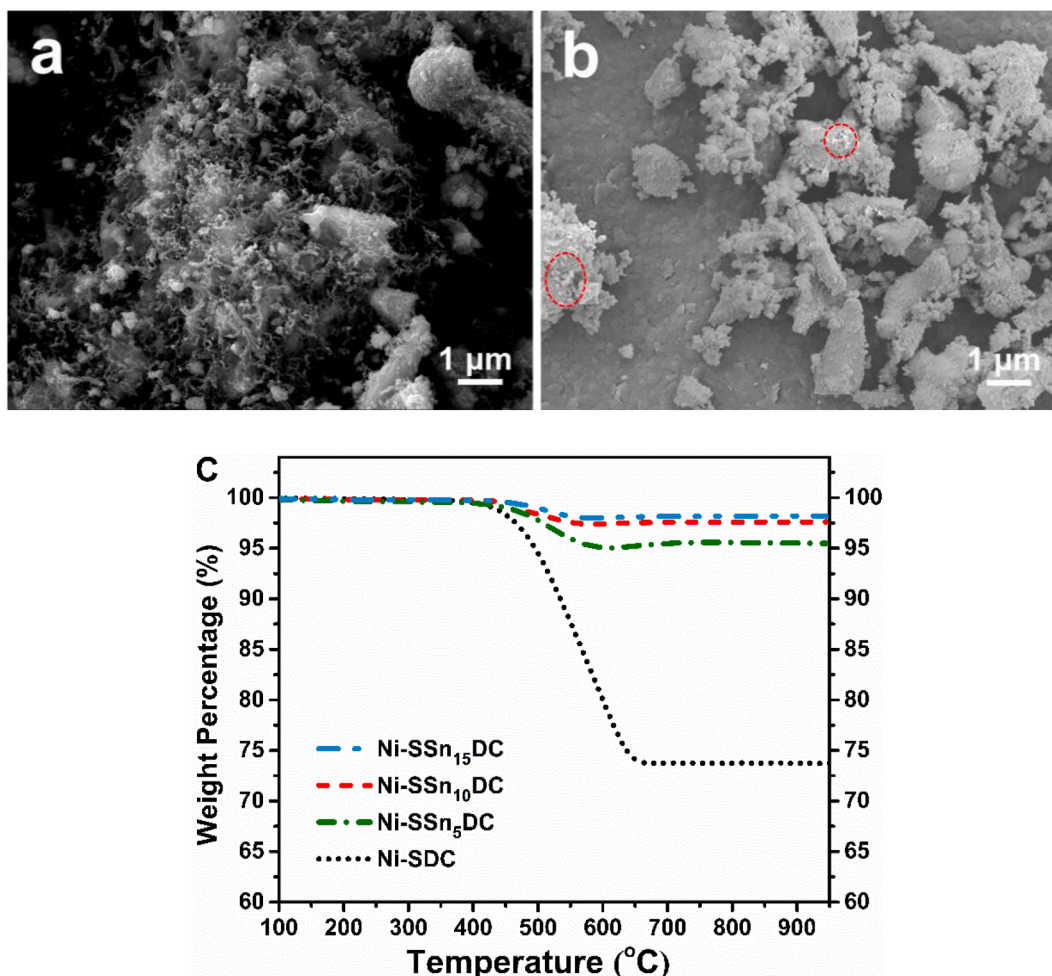


Fig. 6. SEM images of (a) Ni-SDC and (b) $\text{Ni-SSn}_{10}\text{DC}$ powders after carbon deposition; (c) TGA curves of $\text{Ni-SSn}_x\text{DC}$ anodes after carbon deposition.

4. Discussion

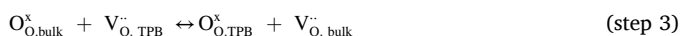
4.1. Electrochemical performance

The performance of the single cell, with a P_{\max} of 2.11 W cm^{-2} at $700 \text{ }^\circ\text{C}$, is a significant improvement on previously reported cells operated below $800 \text{ }^\circ\text{C}$ [18,22,42–45]. It also exhibits superior operational stability when compared with similarly structured SOFCs in the literature [15,46], [47]. Previously reported data can be categorized based on two different strategies: Ni-alloy anodes and oxide doping to the anode support. Our strategy involves coupling the NiSn intermetallic compounds and Sn doped SDC as a composite anode. This composite approach is responsible for the excellent performance. This approach provides an effective example for high-performance hydrocarbon-fueled SOFCs, especially under intermediate operating temperature conditions.

4.2. Reaction mechanism

To design more efficient Ni-based SOFC anodes, it is essential to identify the underlying rate-limiting step of the fuel conversion process. The $\text{CH}_3\text{OH-TPSR}$ results demonstrate that the formation of Ni-Sn intermetallic compounds improves the catalytic activity towards CH_3OH oxidation. However, the reaction mechanism of methanol fuel at SOFC anode is complicated, which involves many reactions such as CH_3OH decomposition, partial/full oxidative reforming, steam reforming, dry-reforming, and electro-oxidation reactions [5]. Therefore, it is difficult to clarify the anode processes with CH_3OH as fuel. Notably, the performance of the single cells exhibit a consistent trend for various anodes when fueled with CH_3OH and H_2 . Therefore, a symmetric cell was examined in detail and the anode reaction mechanism are discussed with using H_2 as the fuel.

The electrochemical oxidation of H_2 at the anode of SOFC starts from the dissociative adsorption of H_2 on the active sites (step (1)), followed by the surface diffusion of the adsorbed H to the reaction site, i.e., the three-phase boundary (TPB, step (2)). Meanwhile, oxygen ions also transfer to TPB in the anode through the ceramic phase (step (3)), which then reacts with the adsorbed H, forming H_2O and releasing electrons (step (4)) [18].



The slope of the fitting straight line should be close to -1 if step (1) is the rate-determining step (RDS) in the anode steps, which will change to -0.5 when the RDS is step (2). The R_p will not change with P_{H_2} if step (3) or (4) is the RDS. The Ni-SDC anode exhibits the lowest slope of -0.31 , and the R_p is more prominent in the LF region of the EIS result (Fig. 1f), implying that the rate of the anode reaction could be codetermined by the surface diffusion of the adsorbed H (step (2)) and the surface reaction between lattice oxygen and the adsorbed H (step (4)).

The electron cloud density of Ni increases with the addition of Sn (Fig. 5a), which may weaken the adsorbing strength of H and accelerate the surface diffusion of H [18], resulting in the decrease of the R_p in the LF region (Fig. 1f) and the increase of the slope (Fig. 1g). Meanwhile, the substitution of Sn for Ce in SDC improves the activity of lattice oxygen (Fig. 5a) and thus accelerates step (4). On the other hand, the doping of Sn may suppress the conduction of O^{2-} in SDC (step (3)), leading to a higher R_p in the HF region (Ni-SSn₁₅DC, Fig. 1f) and the further increase of the slope (Fig. 1g).

Based on above analysis, Sn doped Ni-Ce_{0.8}Sm_{0.2}O_{2- δ} anode clearly displayed improved performance and stability over the Ni-based anode. This fact has two different explanations: (1) The presence of Sn atoms

within the Ni structure, forming Ni₃Sn and Ni₃Sn₂ phase, certainly modifies the electronic density of Ni states, thus affecting its chemistry, which accelerates the surface diffusion of H. (2) The substitution of Sn for Ce in SDC improves the activity of lattice oxygen, which react with the adsorbed H, forming H_2O and releasing electrons. Both the effects of Sn doping in metal and in oxide phases improve the carbon resistance.

5. Conclusions

SSn_xDC is hydrothermally synthesized and investigated as a catalyst precursor of a Ni-based cermet anode. Sn exsolves partially from the ceramic phase after reduction, and Ni₃Sn and Ni₃Sn₂ intermetallic compounds are formed, in which the electrons transfer from Sn to Ni, weakening the adsorbing strength and facilitating the diffusion of H species on the surface of the anode. Meanwhile, the activity of lattice oxygen in the SDC phase, as the support in the composite anode, is also improved with the doping of Sn.

A cell with the Ni-SSn₁₀DC anode yields record high P_{\max} values, e.g., 1.99 and 2.11 W cm^{-2} at $700 \text{ }^\circ\text{C}$ with H_2 and methanol as fuels, respectively. This remarkable performance is superior to the ever-reported Ni-based anodes. Meanwhile, it has been confirmed that the dual modified Ni-SSn_xDC anode are highly resistant to carbon deposition. Such a strategy of anode design may have the great potential of application in the anode material design for non-hydrogen fueled SOFCs, which encounters the great challenge of carbon deposition when the temperature lowers to around $500 \text{ }^\circ\text{C}$, around which selective and stable metal catalyst may be feasible for long term stability.

The surface diffusion of the adsorbed H and the reaction between lattice oxygen and the surface H species are the probable RDS of the anode process, both of which are accelerated with the incorporation of Sn in both the support and metal phases. Ni-SSn₁₀DC anode shows the lowest E_a of 0.32 eV for the electrochemical oxidation of H_2 .

Declaration of Competing Interest

The authors declare that they have no known competing financial interests or personal relationships that could have appeared to influence the work reported in this paper.

Data availability

Data will be made available on request.

Acknowledgements

The financial support from the Program of Introducing Talents to the University Disciplines under file number B06006 and the support of the Program for Changjiang Scholars and Innovative Research Teams in Universities under file number IRT 0641 are gratefully acknowledged. The work has been also supported by the Start-up Fund of Suzhou University of Science and Technology.

Appendix A. Supplementary data

Supplementary data to this article can be found online at <https://doi.org/10.1016/j.cej.2022.140692>.

References

- [1] S. Penner, T. Götsch, B. Klötzer, Increasing complexity approach to the fundamental surface and interface chemistry on sofc anode materials, *Acc. Chem. Res.* 53 (9) (2020) 1811–1821.
- [2] W.C. Chueh, Y. Hao, WooChul Jung, S.M. Haile, High electrochemical activity of the oxide phase in model ceria-Pt and ceria-Ni composite anodes, *Nat. Mater.* 11 (2) (2012) 155–161.
- [3] L. Fan, B. Zhu, P.-C. Su, C. He, Nanomaterials and technologies for low temperature solid oxide fuel cells: recent advances, challenges and opportunities, *Nano Energy* 45 (2018) 148, <https://doi.org/10.1016/j.nanoen.2017.12.044>.

- [4] X.-M. Ge, S.-H. Chan, Q.-L. Liu, Q. Sun, Solid oxide fuel cell anode materials for direct hydrocarbon utilization, *Adv. Energy Mater.* 2 (10) (2012) 1156–1181.
- [5] Q. Xu, M. Ni, Modelling of high temperature direct methanol solid oxide fuel cells, *Int. J. Energy Res.* 45 (2021) 3097–3112, <https://doi.org/10.1002/er.6003>.
- [6] D.R. Palo, R.A. Dagle, J.D. Holladay, Methanol steam reforming for hydrogen production, *Chem. Rev.* 107 (2007) 3992–4021, <https://doi.org/10.1021/cr050198b>.
- [7] P. Wang, H. Cui, C. Wang, Ultrathin PtMo-CeO_x hybrid nanowire assemblies as high-performance multifunctional catalysts for methanol oxidation, oxygen reduction and hydrogen oxidation, *Chem. Eng. J.* 429 (2022), 132435, <https://doi.org/10.1016/j.cej.2021.132435>.
- [8] H. Su, Y.H. Hu, Progress in low-temperature solid oxide fuel cells with hydrocarbon fuels, *Chem. Eng. J.* 402 (2020), 126235, <https://doi.org/10.1016/j.cej.2020.126235>.
- [9] S. McIntosh, R.J. Gorte, Direct hydrocarbon solid oxide fuel cells, *Chem. Rev.* 104 (10) (2004) 4845–4866.
- [10] D. Yoon, A. Manthiram, Hydrogen tungsten bronze as a decoking agent for long-life, natural gas-fueled solid oxide fuel cells, *Energy Environ. Sci.* 7 (2014) 3069, <https://doi.org/10.1039/c4ee01455c>.
- [11] K.S. Blinn, H. Abernathy, X. Li, M. Liu, L.A. Bottomley, M. Liu, Raman spectroscopic monitoring of carbon deposition on hydrocarbon-fed solid oxide fuel cell anodes, *Energy Environ. Sci.* 5 (2012) 7913, <https://doi.org/10.1039/c2ee21499g>.
- [12] L. Yang, Y. Choi, W. Qin, H. Chen, K. Blinn, M. Liu, P. Liu, J. Bai, T.A. Tyson, M. Liu, Promotion of water-mediated carbon removal by nanostructured barium oxide/nickel interfaces in solid oxide fuel cells, *Nat. Commun.* 2 (2011) 357, <https://doi.org/10.1038/ncomms1359>.
- [13] X. Yao, L. Fan, T. Gan, N. Hou, P. Li, Y. Zhao, Y. Li, Coking-resistant NbO_x-Ni-Ce_{0.8}Sm_{0.2}O_{1.9} anode material for methanol-fueled solid oxide fuel cells, *Int. J. Hydrogen Energy* 43 (28) (2018) 12748–12755.
- [14] O. Kwon, K. Kim, S. Joo, H.Y. Jeong, J. Shin, J.W. Han, S. Sengodan, G. Kim, Self-assembled alloy nanoparticles in a layered double perovskite as a fuel oxidation catalyst for solid oxide fuel cells, *J. Mater. Chem. A* 6 (33) (2018) 15947–15953.
- [15] G. Ding, T. Gan, J.i. Yu, P. Li, X. Yao, N. Hou, L. Fan, Y. Zhao, Y. Li, Carbon-resistant Ni_{1-x}Co_x-Ce_{0.8}Sm_{0.2}O_{1.9} anode for solid oxide fuel cells fed with methanol, *Catal. Today* 298 298 (2017) 250–257.
- [16] P. Li, B. Yu, J. Li, X. Yao, Y. Zhao, Y. Li, Improved activity and stability of Ni-Ce_{0.8}Sm_{0.2}O_{1.9} anode for solid oxide fuel cells fed with methanol through addition of molybdenum, *J. Power Sources* 320 (2016) 251–256.
- [17] Z. Du, H. Zhao, S. Yi, Q. Xia, Y. Gong, Y. Zhang, X. Cheng, Y. Li, L. Gu, K. Świerczek, High-performance anode material Sr 2 FeMo 0.65 Ni 0.35 O 6–8 with in situ exsolved nanoparticle catalyst, *ACS Nano* 10 (9) (2016) 8660–8669.
- [18] X. Zhi, T. Gan, N. Hou, L. Fan, T. Yao, J. Wang, Y. Zhao, Y. Li, ZnO-promoted surface diffusion on NiO-Ce_{0.8}Sm_{0.2}O_{1.9} anode for solid oxide fuel cell, *J. Power Sources* 423 423 (2019) 290–296.
- [19] H. Kan, H. Lee, Sn-doped Ni/YSZ anode catalysts with enhanced carbon deposition resistance for an intermediate temperature SOFC, *Appl. Catal. B: Environ.* 97 (1–2) (2010) 108–114.
- [20] D. Yoon, A. Manthiram, Hydrocarbon-fueled solid oxide fuel cells with surface-modified, hydroxylated Sn/Ni-Ce 0.8 Gd 0.2 O 1.9 heterogeneous catalyst anode, *J. Mater. Chem. A* 2 (40) (2014) 17041–17046.
- [21] E. Nikolla, J. Schwank, S. Lincic, Promotion of the long-term stability of reforming Ni catalysts by surface alloying, *J. Catal.* 250 (1) (2007) 85–93.
- [22] P. Li, Z. Wang, X. Yao, N. Hou, L. Fan, T. Gan, Y. Zhao, Y. Li, J.W. Schwank, Effect of Sn addition on improving the stability of Ni-Ce_{0.8}Sm_{0.2}O_{1.9} anode material for solid oxide fuel cells fed with dry CH₄, *Catal. Today* 330 330 (2019) 209–216.
- [23] J. Li, Z. Luo, Y. Zuo, J. Liu, T. Zhang, P. Tang, J. Arbiol, J. Llorca, A. Cabot, NiSn bimetallic nanoparticles as stable electrocatalysts for methanol oxidation reaction, *Appl. Catal. B: Environ.* 234 (2018) 10–18, <https://doi.org/10.1016/j.apcatb.2018.04.017>.
- [24] B. Han, K. Zhao, X. Hou, D.-J. Kim, B.-H. Kim, S. Ha, M.G. Norton, Q. Xu, B.-G. Ahn, Ni-(Ce_{0.8x}Ti_x)Sm_{0.2}O_{2.8} anode for low temperature solid oxide fuel cells running on dry methane fuel, *J. Power Sources* 338 (2017) 1–8, <https://doi.org/10.1016/j.jpowsour.2016.11.024>.
- [25] S. Zhai, H. Xie, B. Chen, M. Ni, A rational design of FeNi alloy nanoparticles and carbonate-decorated perovskite as a highly active and coke-resistant anode for solid oxide fuel cells, *Chem. Eng. J.* 430 (2022), 132615, <https://doi.org/10.1016/j.cej.2021.132615>.
- [26] Z. Huang, L. Fan, N. Hou, T. Gan, J. Gan, Y. Zhao, Y. Li, Improved activity of oxygen in Ni-Ce_{0.8}Sm_{0.2}O_{2.8} anode for solid oxide fuel cell with Pr doping, *J. Power Sources* 451 451 (2020) 227809.
- [27] Y. Zhang, Z. Huang, T. Gan, N. Hou, L. Fan, X. Zhou, G.e. Gao, J. Li, Y. Zhao, Y. Li, Cu-Ce_{0.8}Sm_{0.2}O_{2.8} anode for electrochemical oxidation of methanol in solid oxide fuel cell, *Solid State Ionics* 369 (2021) 115728.
- [28] J.L. Ayastuy, A. Iglesias-González, M.A. Gutiérrez-Ortiz, Synthesis and characterization of low amount tin-doped ceria (Ce_xSn_{1-x}O_{2-δ}) for catalytic CO oxidation, *Chem. Eng. J.* 244 (2014) 372, <https://doi.org/10.1016/j.cej.2014.01.077>.
- [29] T.Y. Kardash, E.A. Derevyannikova, E.M. Slavinskaya, A.I. Stadnichenko, V. A. Maltsev, A.V. Zaikovskii, S.A. Novopashin, A.I. Boronin, K.M. Neyman, Pt/CeO₂ and Pt/CeSnO_x catalysts for low-temperature CO Oxidation prepared by plasma-arc technique, *Frontiers Chem.* 7 (2019) 114, <https://doi.org/10.3389/fchem.2019.00114>.
- [30] Y.u. Chen, B. deGlee, Y.u. Tang, Z. Wang, B. Zhao, Y. Wei, L. Zhang, S. Yoo, K. Pei, J.H. Kim, Y. Ding, P. Hu, F.F. Tao, M. Liu, A robust fuel cell operated on nearly dry methane at 500 °C enabled by synergistic thermal catalysis and electrocatalysis, *Nat. Energy* 3 (12) (2018) 1042–1050.
- [31] U.M. Bhatta, I.M. Ross, T.X.T. Sayle, D.C. Sayle, S.C. Parker, D. Reid, S. Seal, A. Kumar, G. Möbus, Cationic surface reconstructions on cerium oxide nanocrystals: an aberration-corrected hrtem study, *ACS Nano* 6 (1) (2012) 421–430.
- [32] T. Gan, X. Fan, Y.e. Liu, C. Wang, H. Mei, L. Fan, N. Hou, Y. Zhao, Y. Li, A highly active Ni/Ce 0.8 Sm 0.2 O 1.9 anode catalyst with a three-dimensionally ordered macroporous structure for solid oxide fuel cells, *J. Mater. Chem. A* 8 (16) (2020) 7792–7800.
- [33] X. Yao, Q. Yu, Z. Ji, Y. Lv, Y. Cao, C. Tang, F. Gao, L. Dong, Y.i. Chen, A comparative study of different doped metal cations on the reduction, adsorption and activity of CuO/Ce_{0.67}M_{0.33}O₂ (M=Zr⁴⁺, Sn⁴⁺, Ti⁴⁺) catalysts for NO+CO reaction, *Appl. Catal. B: Environ.* 130–131 (2013) 293–304.
- [34] X. Zhu, X. Gao, R. Qin, Y. Zeng, R. Qu, C. Zheng, X. Tu, Plasma-catalytic removal of formaldehyde over Cu-Ce catalysts in a dielectric barrier discharge reactor, *Appl. Catal. B: Environ.* 170 (2015) 293, <https://doi.org/10.1016/j.apcatb.2015.01.032>.
- [35] X. Yao, Y. Xiong, W. Zou, L. Zhang, S. Wu, X. Dong, F. Gao, Y.u. Deng, C. Tang, Z. Chen, L. Dong, Y.i. Chen, Correlation between the physicochemical properties and catalytic performances of Ce_xSn_{1-x}O₂ mixed oxides for NO reduction by CO, *Appl. Catal. B: Environ.* 144 (2014) 152–165.
- [36] C. Liu, H. Xian, Z. Jiang, L. Wang, J. Zhang, L. Zheng, Y. Tan, X. Li, Insight into the improvement effect of the Ce doping into the SnO₂ catalyst for the catalytic combustion of methane, *Appl. Catal. B: Environ.* 176 (2015) 542, <https://doi.org/10.1016/j.apcatb.2015.04.042>.
- [37] R.-P. Ye, Q. Li, W. Gong, T. Wang, J.J. Razink, L. Lin, Y.-Y. Qin, Z. Zhou, H. Adidharma, J. Tang, A.G. Russell, M. Fan, Y.-G. Yao, High-performance of nanostructured Ni/CeO₂ catalyst on CO₂ methanation, *Appl. Catal. B: Environ.* 268 (2020) 118474.
- [38] X. Liu, X. Liu, G. Xu, Y. Zhang, C. Wang, Q. Lu, L. Ma, Highly efficient catalytic conversion of cellulose into acetol over Ni-Sn supported on nanosilica and the mechanism study, *Green Chem.* 21 (20) (2019) 5647–5656.
- [39] C.-S. Chen, C.S. Budi, H.-C. Wu, D. Saikia, H.-M. Kao, Size-tunable Ni nanoparticles supported on surface-modified, cage-type mesoporous silica as highly active catalysts for CO₂ hydrogenation, *ACS Catal.* 7 (12) (2017) 8367–8381.
- [40] Q. Liu, Z. Zhong, F. Gu, X. Wang, X. Lu, H. Li, G. Xu, F. Su, CO methanation on ordered mesoporous Ni-Cr-Al catalysts: effects of the catalyst structure and Cr promoter on the catalytic properties, *J. Catal.* 337 (2016) 221, <https://doi.org/10.1016/j.jcat.2016.01.023>.
- [41] R. Sun, M. Zheng, J. Pang, X. Liu, J. Wang, X. Pan, A. Wang, X. Wang, T. Zhang, Selectivity-switchable conversion of cellulose to glycols over ni-sn catalysts, *ACS Catal.* 6 (1) (2016) 191–201.
- [42] M. Akbi, A. Lefort, Work function measurements of contact materials for industrial use, *J. Phys. D: Appl. Phys.* 31 (11) (1998) 1301–1308.
- [43] E. Nikolla, J. Schwank, S. Lincic, Comparative study of the kinetics of methane steam reforming on supported Ni and Sn/Ni alloy catalysts: the impact of the formation of Ni alloy on chemistry, *J. Catal.* 263 (2) (2009) 220–227.
- [44] E. Nikolla, A. Holewinski, J. Schwank, S. Lincic, Controlling carbon surface chemistry by alloying: carbon tolerant reforming catalyst, *J. Am. Chem. Soc.* 128 (2006) 11354, <https://doi.org/10.1021/ja0638298>.
- [45] I.V. Yentekakis, P. Panagiotopoulou, G. Artemakis, A review of recent efforts to promote dry reforming of methane (DRM) to syngas production via bimetallic catalyst formulations, *Appl. Catal. B: Environ.* 296 (2021), 120210, <https://doi.org/10.1016/j.apcatb.2021.120210>.
- [46] T. Gan, G. Ding, X. Zhi, L. Fan, N. Hou, X. Yao, P. Li, Y. Zhao, Y. Li, A LaNi_{0.9}Co_{0.1}O₃ coated Ce_{0.8}Sm_{0.2}O_{1.9} composite anode for solid oxide fuel cells fed with methanol, *Catal. Today* 327 (2019) 220–225, <https://doi.org/10.1016/j.cattod.2018.04.050>.